International Journal of Solids and Structures 100–101 (2016) 127–137

Contents lists available at ScienceDirect

International Journal of Solids and Structures

journal homepage: www.elsevier.com/locate/ijsolstr

Rigid-plastic torsion of a hollow tube in strain-gradient plasticity

Vlado A. Lubarda*

Departments of NanoEngineering and Mechanical and Aerospace Engineering, University of California, San Diego, La Jolla, CA 92093-0448, USA

ARTICLE INFO

Article history:
Available online 5 September 2016

Keywords:
Hollow tube
Material length parameter
Microstress
Moment-stress
Principle of virtual work
Rigid-plastic
Strain-gradient plasticity
Torsion

ABSTRACT

Closed-form expressions for the Cauchy stress, microstress, moment-stress, and the torque-twist relationship in a twisted hollow circular tube are derived for a rigid-plastic strain-gradient plasticity. This is accomplished for any of the gradient-enhanced effective plastic strain measures from a considered broad class of these measures. Numerical results are given and discussed for the two most frequently utilized measures and for the three adopted stress-strain relationships modeling the uniaxial tension test. Solid circular rods and thin-walled tubes are both considered. The existence of the line forces is also discussed from the standpoint of the basic equilibrium considerations and the principle of virtual work.

1. Introduction

In the wake of Fleck and Hutchinson (1993) and Fleck et al. (1994) analyzes of the effects of strain-gradient on plastic response of materials at micron scale, there has been a great amount of research devoted to the development of what is now known as the strain-gradient plasticity. The representative references include, inter alia, the contributions by Fleck and Hutchinson (1997, 2001); Nix and Gao (1998); Gao et al. (1999); Huang et al. (2000, 2004); Hutchinson (2000, 2012); Gurtin (2002, 2003, 2004); Gudmundson (2004); Anand et al. (2005a); Gurtin and Anand (2005a, 2005b, 2009); Bardella (2006, 2007); Fleck and Willis (2009a, 2009b); Polizzotto (2009); Voyiadjis et al. (2010); Dahlberg et al. (2013); Nielsen and Niordson (2014); Fleck et al. (2014, 2015); Bardella and Panteghini (2015); Anand et al. (2015b). In most of these works the material length parameter is introduced in the theory through the definition of the gradient-enhanced effective plastic strain, which combines the contributions from the effective plastic strain and the effective plastic strain-gradient. Physically, the size-dependence in non-uniform deformation problems at micron scale has been attributed to the existence of large gradients of plastic strain and the associated network of the so-called geometrically necessary dislocations. The increase of the plastic collapse limit load with the decreasing specimen size was pointed out and elaborated upon by Polizzotto (2010, 2011).

The objective of the present paper is to derive the complete stress field (microstress, moment-stress, and the Cauchy stress) and the torque-twist relationship for a twisted hollow circular tube made of a rigid-plastic material by using any of the gradient-enhanced effective plastic strain measures from a wide class of these measures frequently adopted in the literature. Special attention is given to measures defined by the linear and harmonic sum of the effective plastic strain and its gradient, scaled by the material length. The torsion testing of thin wires was a benchmark problem demonstrating the size effect at micron scale (Fleck et al., 1994), which was further studied, using different constitutive models, by many investigators, including (Fleck and Hutchinson, 1997; Fleck et al., 2014; Huang et al., 2000; Gudmundson, 2004; Voyiadjis and Abu Al-Rub, 2005; Idiart et al., 2009; Polizzotto, 2011; Liu et al., 2013; Lubarda, 2016a). The general results derived in this paper hold for an arbitrary expression representing the stress-plastic strain response in simple tension, although numerical evaluations are performed by adopting three specific expressions.

2. Gradient-enhanced effective plastic strain

In a simple formulation of the deformation theory of strain-gradient plasticity (Hutchinson, 2012), the specific plastic work (per unit volume) is expressed in terms of the gradient-enhanced effective plastic strain E_p by

$$w_p(E_p) = \int_0^{E_p} \sigma_0(\epsilon_p)\, d\epsilon_p\,, \tag{1}$$

where $\sigma_0 = \sigma_0(\epsilon_p)$ represents the stress-strain curve from the uniaxial tension test. The expression (1) implies that the plastic work needed to deform the material element in the presence of strain-gradients is equal to that at the same strain in the absence of gradients.

* Fax: +1 858 534 5698.
E-mail address: vlubarda@ucsd.edu

http://dx.doi.org/10.1016/j.ijsolstr.2016.07.029
0020-7683/

A wide class of the gradient-enhanced effective plastic strain measures, each involving one material length parameter l, is (Evans and Hutchinson, 2009; Fleck and Hutchinson, 1997)

$$E_{\rm p} = \left(e_{\rm p}^s + l^s g_{\rm p}^s\right)^{1/s}, \quad (s \geq 1), \tag{2}$$

where $e_{\rm p}$ is the effective plastic strain and $g_{\rm p}$ the effective plastic strain-gradient, defined by

$$e_{\rm p} = \left(\frac{2}{3}\epsilon_{ij}^{\rm p}\epsilon_{ij}^{\rm p}\right)^{1/2}, \quad g_{\rm p} = \left(\frac{2}{3}\epsilon_{ij,k}^{\rm p}\epsilon_{ij,k}^{\rm p}\right)^{1/2}. \tag{3}$$

The two most frequently used measures are associated with the choices $s = 1$ and $s = 2$, which specify $E_{\rm p}$ as either a linear or harmonic sum of $e_{\rm p}$ and $lg_{\rm p}$,

$$E_{\rm p} = e_{\rm p} + lg_{\rm p}, \quad E_{\rm p} = \left(e_{\rm p}^2 + l^2 g_{\rm p}^2\right)^{1/2}. \tag{4}$$

In general, when fitting experimental data, a different value of l may be needed for each choice of s. The choice $s = 2$ is particulary appealing from the mathematical point of view and was used in most studies of the strain-gradient plasticity, although in some studies the choice $s = 1$ was found to be more attractive (Evans and Hutchinson, 2009).

The plastic strain is taken to be

$$\epsilon_{ij}^{\rm p} = e_{\rm p} m_{ij}, \quad m_{ij} = \frac{3}{2}\frac{\sigma_{ij}'}{\sigma_{\rm eq}}, \tag{5}$$

where the equivalent stress is

$$\sigma_{\rm eq} = \left(\frac{3}{2}\sigma_{ij}'\sigma_{ij}'\right)^{1/2}, \tag{6}$$

with the prime designating a deviatoric part. The total infinitesimal strain is

$$\epsilon_{ij} = \epsilon_{ij}^{\rm e} + \epsilon_{ij}^{\rm p}, \tag{7}$$

with the elastic component related to the Cauchy stress by the isotropic generalized Hooke's law

$$\epsilon_{ij}^{\rm e} = \frac{1}{2\mu}\sigma_{ij}' + \frac{1}{9\kappa}\sigma_{kk}\delta_{ij}, \quad \sigma_{ij}' = \sigma_{ij} - \frac{1}{3}\sigma_{kk}\delta_{ij}. \tag{8}$$

The shear and bulk moduli are μ and κ.

3. Work-conjugates to plastic strain and its gradient

It is assumed that plastic strain-gradients $\epsilon_{ij,k}^{\rm p}$ contribute to the work per unit volume. The work conjugate to $\epsilon_{ij,k}^{\rm p}$ is the moment-stress $\tau_{ijk} = \tau_{jik}$. The work-conjugate to $\epsilon_{ij}^{\rm p}$ is the microstress $q_{ij} = q_{ji}$, such that (Gudmundson, 2004)

$$\dot{w}_{\rm p} = q_{ij}\dot{\epsilon}_{ij}^{\rm p} + \tau_{ijk}\dot{\epsilon}_{ij,k}^{\rm p}. \tag{9}$$

To identify q_{ij} and τ_{ijk}, we reconcile (9) with the rate of plastic work expression

$$\dot{w}_{\rm p} = \sigma_0(E_{\rm p})\dot{E}_{\rm p}, \tag{10}$$

following from (1). Since, by the differentiation of (2) and (3),

$$\dot{E}_{\rm p} = E_{\rm p}^{1-s}\left(e_{\rm p}^{s-1}\dot{e}_{\rm p} + l^s g_{\rm p}^{s-1}\dot{g}_{\rm p}\right), \tag{11}$$

and

$$\dot{e}_{\rm p} = \frac{2}{3e_{\rm p}}\epsilon_{ij}^{\rm p}\dot{\epsilon}_{ij}^{\rm p}, \quad \dot{g}_{\rm p} = \frac{2}{3g_{\rm p}}\epsilon_{ij,k}^{\rm p}\dot{\epsilon}_{ij,k}^{\rm p}, \tag{12}$$

we obtain

$$\dot{E}_{\rm p} = \frac{2}{3}E_{\rm p}^{1-s}\left(e_{\rm p}^{s-2}\epsilon_{ij}^{\rm p}\dot{\epsilon}_{ij}^{\rm p} + l^s g_{\rm p}^{s-2}\epsilon_{ij,k}^{\rm p}\dot{\epsilon}_{ij,k}^{\rm p}\right). \tag{13}$$

The substitution of (13) into (10) and the comparison with (9) establishes, up to their workless terms, the work-conjugates

$$q_{ij} = \frac{2}{3}\frac{\sigma_0(E_{\rm p})}{E_{\rm p}^{s-1}}e_{\rm p}^{s-2}\epsilon_{ij}^{\rm p}, \quad \tau_{ijk} = \frac{2}{3}l^s\frac{\sigma_0(E_{\rm p})}{E_{\rm p}^{s-1}}g_{\rm p}^{s-2}\epsilon_{ij,k}^{\rm p}. \tag{14}$$

Clearly, $q_{ii} = 0$ and $\tau_{iik} = 0$, because $\epsilon_{ii}^{\rm p} = 0$. Expressions (14) can also be deduced directly from $q_{ij} = \partial w_{\rm p}/\partial\epsilon_{ij}^{\rm p} = \sigma_0\partial E_{\rm p}/\partial\epsilon_{ij}^{\rm p}$ and $\tau_{ijk} = \partial w_{\rm p}/\partial\epsilon_{ij,k}^{\rm p} = \sigma_0\partial E_{\rm p}/\partial\epsilon_{ij,k}^{\rm p}$, as done by Liu et al. (2013).

In particular, for $s = 1$, the microstress and the moment-stress are

$$q_{ij} = \frac{2}{3}\frac{\sigma_0(E_{\rm p})}{e_{\rm p}}\epsilon_{ij}^{\rm p}, \quad \tau_{ijk} = \frac{2}{3}l\frac{\sigma_0(E_{\rm p})}{g_{\rm p}}\epsilon_{ij,k}^{\rm p}, \tag{15}$$

while for $s = 2$,

$$q_{ij} = \frac{2}{3}\frac{\sigma_0(E_{\rm p})}{E_{\rm p}}\epsilon_{ij}^{\rm p}, \quad \tau_{ijk} = \frac{2}{3}l\frac{\sigma_0(E_{\rm p})}{E_{\rm p}}\epsilon_{ij,k}^{\rm p}. \tag{16}$$

4. Principle of virtual work

The principle of virtual work of strain-gradient plasticity reads (Gudmundson, 2004; Gurtin and Anand, 2005a, 2005b; Fleck et al., 2014)

$$\int_V (\sigma_{ij}\delta\epsilon_{ij}^{\rm e} + q_{ij}\delta\epsilon_{ij}^{\rm p} + \tau_{ijk}\delta\epsilon_{ij,k}^{\rm p})\mathrm{d}V = \int_S (T_i\delta u_i + t_{ij}\delta\epsilon_{ij}^{\rm p})\mathrm{d}S, \tag{17}$$

provided that the equations of equilibrium hold

$$\sigma_{ij,j} = 0, \quad \tau_{ijk,k} + \sigma_{ij}' - q_{ij} = 0, \tag{18}$$

and the traction-stress relations

$$T_i = \sigma_{ij}n_j, \quad t_{ij} = \tau_{ijk}n_k \tag{19}$$

between the traction vector T_i and the Cauchy stress tensor σ_{ij}, and between the (deviatoric) moment-traction tensor t_{ij} are the moment-stress tensor τ_{ijk}. The components of the outward unit vector, orthogonal to the considered surface element, are denoted by n_i. The displacement components are u_i.

In the case of a rigid-plastic material, the principle of virtual work reads

$$\int_V \left(q_{ij}'\delta\epsilon_{ij}^{\rm p} + \tau_{ijk}'\delta\epsilon_{ij,k}^{\rm p} + \frac{1}{3}\sigma_{ii}\delta\epsilon_{jj}^{\rm p}\right)\mathrm{d}V = \int_S \left[\hat{T}_i\delta u_i + \hat{R}_i D(\delta u_i)\right]\mathrm{d}S. \tag{20}$$

The three independent traction components $\hat{T}_i$ are

$$\hat{T}_i = \bar{T}_i - n_i n_j R_j(D_k n_k) - D_i(n_j R_j), \tag{21}$$

with

$$\bar{T}_i = T_i + R_i(D_j n_j) - D_j t_{ij}, \quad T_i = \sigma_{ij}n_j, \tag{22}$$

while the two independent higher-order traction components $\hat{R}_i$, tangential to S, are

$$\hat{R}_i = R_i - n_i n_j R_j, \quad R_i = t_{ij}n_j, \tag{23}$$

with $t_{ij} = \tau_{ijk}'n_j n_k$. The utilized surface gradient operator is defined by $D_i = (\partial/\partial x_i) - n_i D$, where D is the projection of the gradient operator to the surface normal, $D = n_j(\partial/\partial x_j)$. The spherical component of Cauchy stress $\sigma_{ii}/3$ was used in (20) as the Lagrange multiplier, associated with the incompressibility constraint $\epsilon_{jj}^{\rm p} = 0$ (Fleck and Willis, 2009b).

If the surface S has edges, an additional term appears on the right-hand side of (20), given by

$$\sum_n \oint_{C_n} p_i\delta u_i\,\mathrm{d}C_n, \tag{24}$$

where p_i are the line forces along the edges C_n of the smooth parts S_n of a piece-wise smooth surface S. For example, the line force along an edge formed by the intersection of two smooth surface segments $S^{(1)}$ and $S^{(2)}$ is

$$p_i = \left[\tau_{ijk}'k_j^{(1)}n_k^{(1)} - k_i^{(1)}\tau_{jkl}'n_j^{(1)}n_k^{(1)}n_l^{(1)}\right] + \left[\tau_{ijk}'k_j^{(2)}n_k^{(2)} - k_i^{(2)}\tau_{jkl}'n_j^{(2)}n_k^{(2)}n_l^{(2)}\right], \tag{25}$$

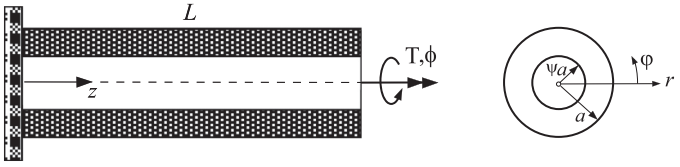

Fig. 1. A hollow circular tube of length L under applied torque T. The angle of rotation of the end $z = L$ relative to the fixed end is ϕ. The outer radius of the tube is a, and the inner radius is ψa ($0 \le \psi < 1$). The utilized cylindrical coordinates are (r, φ, z).

where $\mathbf{n}^{(i)}$ is the unit outward normal to surface $S^{(i)}$ $(i = 1, 2)$, and $\mathbf{k}^{(i)} = \mathbf{c}^{(i)} \times \mathbf{n}^{(i)}$. The vector $\mathbf{c}^{(i)}$ is the unit tangent vector along the intersecting edge of the two surfaces with $S^{(i)}$ to the left. The first subscript in τ_{ijk} specifies the normal to the surface over which the τ_{ijk} component acts, the second index specifies the orientation of the forces, and the third index specifies the orientation of the lever arm between the two forces of the doublet. Details of the derivation are given in the appendix of the paper.

5. Torsion of a hollow circular tube

The effects of strain-gradients on plastic response have been studied for various problems at micron scale, including bending and torsion of thin beams and wires, plastic void growth, and indentation hardness testing (Fleck et al., 1994; Fleck and Hutchinson, 1997, 2001; Stölken and Evans, 1998; Gao et al., 1999; Nix and Gao, 1998; Huang et al., 2000; Gudmundson, 2004; Voyiadjis and Abu Al-Rub, 2005; Idiart et al., 2009; Liu et al., 2013). We consider in this section a torsion of a hollow circular tube made of a rigid-plastic material. This is appealing because the problem allows the derivation of the closed-form analytical expressions for the stress and moment-stress fields for any choice of s in the definition of the gradient-enhanced effective plastic strain (2), and for any assumed stress-strain relation in uniaxial tension test $\sigma_0 = \sigma_0(\epsilon_p)$. It also allows a deduction of the solutions for a solid rod and a thin-walled tube as special cases.

The outer radius of the tube is denoted by a and the inner radius by ψa, where $0 \le \psi < 1$. The applied torque is denoted by T and the corresponding angle of rotation (relative to the fixed end) by $\phi(L)$, where L is the length of the tube (Fig. 1). If the applied torque $T > T_Y$, the non-vanishing strain components are

$$\epsilon_{z\varphi} = \epsilon_{\varphi z} = \frac{r\theta}{2}\,, \quad (\theta = \mathrm{d}\phi/\mathrm{d}z)\,, \tag{26}$$

where θ is the angle of twist (per unit length of the tube), and (r, φ, z) are the cylindrical coordinates with z along the central axis of the tube. The corresponding strain tensor is

$$\boldsymbol{\epsilon} = \epsilon_{z\varphi}(\mathbf{i}_z \otimes \mathbf{i}_\varphi + \mathbf{i}_\varphi \otimes \mathbf{i}_z)\,, \tag{27}$$

where $(\mathbf{i}_r, \mathbf{i}_\varphi, \mathbf{i}_z)$ are the unit vectors of the cylindrical coordinate system, and $\otimes$ designates the tensor product. Recalling that the gradient operator in cylindrical coordinates is $\boldsymbol{\nabla} = \mathbf{i}_r(\partial/\partial r) + \mathbf{i}_\varphi r^{-1}(\partial/\partial\varphi) + \mathbf{i}_z(\partial/\partial z)$, and that $\partial\mathbf{i}_r/\partial\varphi = \mathbf{i}_\varphi$ and $\partial\mathbf{i}_\varphi/\partial\varphi = -\mathbf{i}_r$, the strain-gradient tensor is found to be

$$\boldsymbol{\gamma} = \boldsymbol{\epsilon}\boldsymbol{\nabla} = \frac{\partial\epsilon_{z\varphi}}{\partial r}(\mathbf{i}_z \otimes \mathbf{i}_\varphi + \mathbf{i}_\varphi \otimes \mathbf{i}_z) \otimes \mathbf{i}_r - \frac{\epsilon_{z\varphi}}{r}(\mathbf{i}_z \otimes \mathbf{i}_r + \mathbf{i}_r \otimes \mathbf{i}_z) \otimes \mathbf{i}_\varphi\,, \tag{28}$$

with the nonvanishing physical components

$$\gamma_{z\varphi r} = \gamma_{\varphi zr} = \frac{\partial\epsilon_{z\varphi}}{\partial r} = \frac{\theta}{2}\,, \quad \gamma_{zr\varphi} = \gamma_{rz\varphi} = -\frac{\epsilon_{z\varphi}}{r} = -\frac{\theta}{2}\,. \tag{29}$$

Since elastic component of strain is absent in the case of a rigid-plastic model, there is no deformation for $T \le T_Y$, while for $T > T_Y$ the entire deformation is plastic. The expression for T_Y will be derived in the sequel. Assuming proportional straining and the framework of the deformation theory of strain-gradient plasticity from Sections 2–4, we find from (3)

$$e_p = \left(\frac{2}{3}\epsilon_{ij}\epsilon_{ij}\right)^{1/2} = \frac{r\theta}{\sqrt{3}}\,, \quad g_p = \left(\frac{2}{3}\gamma_{ijk}\gamma_{ijk}\right)^{1/2} = \sqrt{\frac{2}{3}}\,\theta\,. \tag{30}$$

Upon the substitution of (30) into (2), the gradient-enhanced effective plastic strain and its gradient are found to be

$$E_p = \frac{\theta}{\sqrt{3}}\left[r^s + (\sqrt{2}l)^s\right]^{1/s}, \quad E_{p,r} = E_p\,\frac{r^{s-1}}{r^s + (\sqrt{2}l)^s}\,. \tag{31}$$

This type of expression for E_p was also derived in the analysis of wire torsion by Liu et al. (2013); see their equation (43). The plots of E_p vs. r along the radius of a twisted solid rod for three selected values of s and two values of the material length l are shown in Fig. 2. For any θ, the entire contribution to E_p at the center of a solid rod is from the strain-gradient. As r increases the strain contribution increases, while the strain-gradient contribution remains constant. If $l \ll a$, the strain contribution in the outer portion of the rod (near $r = a$) is a dominant contribution to E_p.

The microstress and the moment-stress components can be determined by introducing (31) into (14), with the results

$$q_{z\varphi} = \frac{\sigma_0(E_p)}{\sqrt{3}}\,\frac{r^{s-1}}{[r^s + (\sqrt{2}l)^s]^{1-1/s}}\,, \tag{32}$$

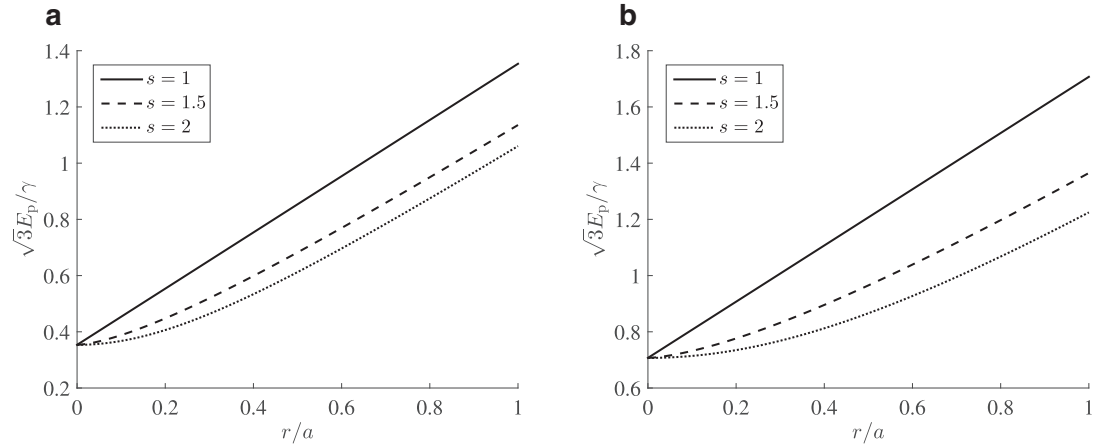

Fig. 2. The variation of the gradient-enhanced effective plastic strain E_p (normalized by $\gamma/\sqrt{3}$, where $\gamma = a\theta$ is the surface shear strain), along the radius of a twisted rod, according to (30), for three different values of s. In part (a) the material length $l = a/4$, and in part (b) $l = a/2$.

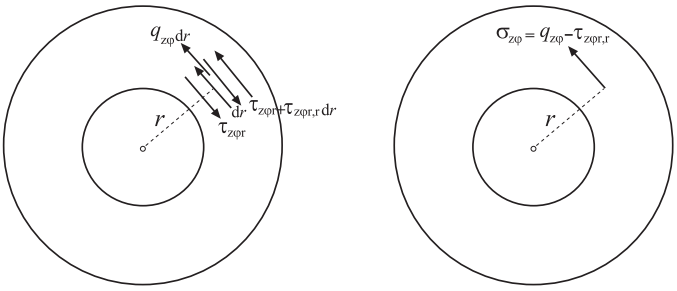

Fig. 3. Physical interpretation of the relationship between the Cauchy stress $\sigma_{z\varphi}$, the microstress $q_{z\varphi}$, and the moment-stress $\tau_{z\varphi r}$. The microstress $q_{z\varphi}$ and the gradient of the moment-stress $\tau_{z\varphi r,\,r}$ combine to give the Cauchy stress $\sigma_{z\varphi}=q_{z\varphi}-\tau_{z\varphi r,r}$.

$$\tau_{z\varphi r}=\frac{1}{2}\,\frac{(\sqrt{2}l)^s}{r^{s-1}}\,q_{z\varphi}=\frac{1}{2}\,\frac{\sigma_0(E_{\rm p})}{\sqrt{3}}\,\frac{(\sqrt{2}l)^s}{[r^s+(\sqrt{2}l)^s]^{1-1/s}},$$
$$\tau_{zr\varphi}=-\tau_{z\varphi r}\,. \tag{33}$$

The Cauchy stress follows from the second of the equilibrium conditions in (17) as

$$\sigma_{z\varphi}=q_{z\varphi}-\tau_{z\varphi r,r}\,. \tag{34}$$

Upon evaluating $\tau_{z\varphi r,\,r}$ from (33) and using (32), Eq. (34) gives

$$\sigma_{z\varphi}=\left[1-\frac{1}{2}\,\frac{(\sqrt{2}l)s}{r^s+(\sqrt{2}l)^s}\left(1-s+\frac{E_{\rm p}}{\sigma_0}\,\frac{{\rm d}\sigma_0}{{\rm d}E_{\rm p}}\right)\right]q_{z\varphi}\,, \tag{35}$$

i.e.,

$$\sigma_{z\varphi}=\frac{\sigma_0(E_{\rm p})}{\sqrt{3}}\,\frac{r^{s-1}}{[r^s+(\sqrt{2}l)^s]^{2-1/s}}\left[r^s+\frac{1}{2}\,(\sqrt{2}l)^s\left(1+s-\frac{E_{\rm p}}{\sigma_0}\,\frac{{\rm d}\sigma_0}{{\rm d}E_{\rm p}}\right)\right]. \tag{36}$$

In addition, from (25), the circumferential line force along the outer radius $r=a$ of the cross-section of the tube is $p_\varphi=\tau_{z\varphi r}(a)$, while $p_\varphi=-\tau_{z\varphi r}(\psi a)$ along the inner radius $r=\psi a$. Physically, these line forces are the consequence of the fact that within the cross-section of the tube the adjacent moment-stress components ($\tau_{z\varphi r}$ and $\tau_{z\varphi r}+\tau_{z\varphi r,r}{\rm d}r$) combine at each point along the radius r with the microstress $q_{z\varphi}$ to give the Cauchy stress $\sigma_{z\varphi}=q_{z\varphi}-\tau_{z\varphi r,r}$ (Fig. 3), except at the end points of the cross-section $r=a$ and $r=\psi a$, where $\tau_{z\varphi r}$ is left unpaired. This gives rise to concentrated line forces p_φ along the edges $r=a$ and $r=\psi a$. Thus, within each cross-section of the tube, the Cauchy stress/line force system ($\sigma_{z\varphi}$, p_φ) is equipollent to the microstress/moment-stress system ($q_{z\varphi}$, $\tau_{z\varphi r}$, $\tau_{zr\varphi}$), both systems being statically equivalent to the applied torque T. If the actual application of the torque at the end $z=L$ is different from that predicted by the solution, the Saint–Venant's principle can be invoked and the derived solution applies sufficiently away from the end.

The existence of the concentrated line forces is a peculiar feature of the adopted rigid-plastic strain-gradient material model. If the elastic-plastic model was adopted instead, the line forces would not appear, as elaborated in great detail by Engelen et al. (2006) in their analysis of beam bending. They showed that the elastoplastic solution reproduces the rigid-plastic solution in the limit when the modulus of elasticity $E\to\infty$. The rapidly increasing elastoplastic stress in the boundary layer near the edges gives rise to line forces in the rigid-plastic limit.

5.1. Results for $s=1$ and $s=2$

For $s=1$, the derived expressions simplify to

$$q_{z\varphi}=\frac{\sigma_0(E_{\rm p})}{\sqrt{3}}\,,\quad E_{\rm p}=\frac{\theta}{\sqrt{3}}\,(r+\sqrt{2}l)\,, \tag{37}$$

$$\tau_{z\varphi r}=\frac{lq_{z\varphi}}{\sqrt{2}}=\frac{l\sigma_0(E_{\rm p})}{\sqrt{6}}=-\tau_{zr\varphi}\,, \tag{38}$$

$$\sigma_{z\varphi}=\frac{\sigma_0(E_{\rm p})}{\sqrt{3}}\left(1-\frac{1}{\sqrt{6}}\,\frac{l\theta}{\sigma_0}\,\frac{{\rm d}\sigma_0}{{\rm d}E_{\rm p}}\right). \tag{39}$$

For $s=2$, the results are

$$q_{z\varphi}=\frac{\sigma_0(E_{\rm p})}{\sqrt{3}}\,\frac{r}{(r^2+2l^2)^{1/2}}\,,\quad E_{\rm p}=\frac{\theta}{\sqrt{3}}\,(r^2+2l^2)^{1/2}\,, \tag{40}$$

$$\tau_{z\varphi r}=\frac{l^2q_{z\varphi}}{r}=\frac{\sigma_0(E_{\rm p})}{\sqrt{3}}\,\frac{l^2}{(r^2+2l^2)^{1/2}}=-\tau_{zr\varphi}\,, \tag{41}$$

$$\sigma_{z\varphi}=\frac{\sigma_0(E_{\rm p})}{\sqrt{3}}\,\frac{r}{(r^2+2l^2)^{3/2}}\left(r^2+3l^2-l^2\,\frac{E_{\rm p}}{\sigma_0}\,\frac{{\rm d}\sigma_0}{{\rm d}E_{\rm p}}\right). \tag{42}$$

Fig. 4 shows the variation of the shear stress $\sigma_{z\varphi}$ (black curves) and microstress $q_{z\varphi}$ (red curves) with r/a at three levels of strain $\gamma=a\theta$ for a solid rod of radius a. Part (a) is for $s=1$, and part (b) for $s=2$. The utilized stress-strain relationship $\sigma_0=\sigma_0(E_{\rm p})$ is specified by the first expression in (52), with $m=46.66$ and $n=$

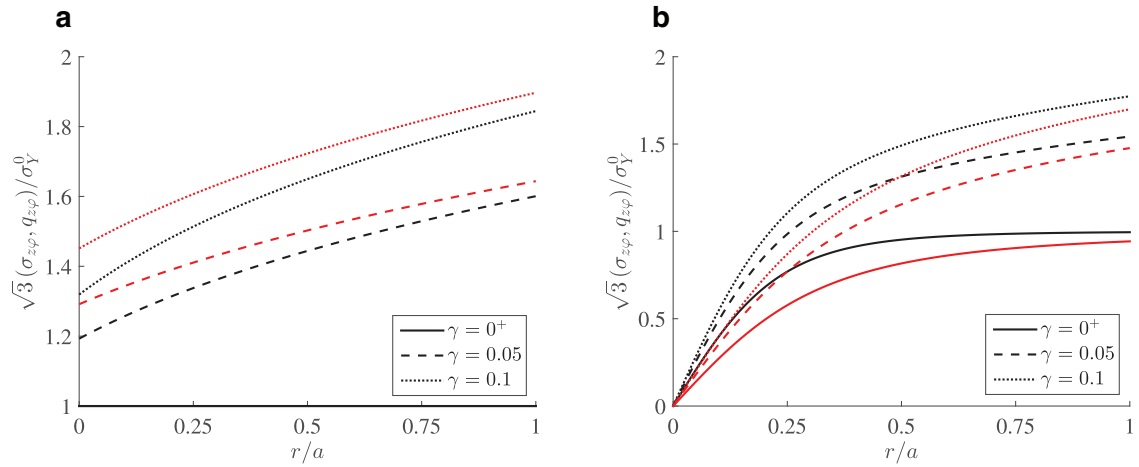

Fig. 4. The variations of $\sigma_{z\varphi}$ (black curves) and $q_{z\varphi}$ (red curves) with r/a at three levels of strain $\gamma=a\theta$ for a solid rod of radius a. The relationship $\sigma_0=\sigma_0(E_{\rm p})$ is specified by the first expression in (52), with $m=46.66$ and $n=0.225$. The material length parameter is $l=a/4$. Part (a) is for $s=1$, and part (b) for $s=2$.

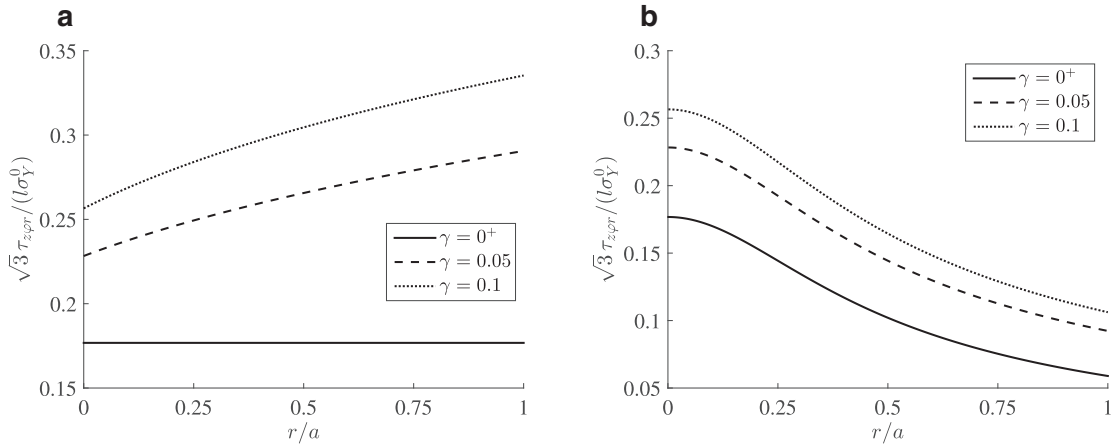

Fig. 5. The variation of $\tau_{z\varphi r}$ with r/a at three levels of strain $\gamma = a\theta$ for a solid rod of radius a and the same data as used in Fig. 4. Part (a) is for $s = 1$, and part (b) for $s = 2$.

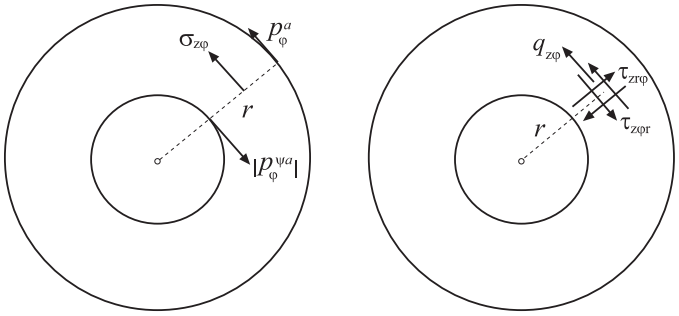

Fig. 6. Two alternative calculations of the torque T from two equipollent systems: (a) $(\sigma_{z\varphi}, p_\varphi)$ and (b) $(q_{z\varphi}, \tau_{z\varphi r}, \tau_{zr\varphi})$.

0.225 (these values are discussed in Section 7). The material length parameter is chosen to be $l = a/4$ for all curves. The corresponding plots of the moment-stress $\tau_{z\varphi r}$ are shown in Fig. 5. For $s = 1$, the moment-stress $\tau_{z\varphi r}$ increases with r (for $\gamma > 0$), while for $s = 2$ the moment-stress $\tau_{z\varphi r}$ is a decreasing function of r, with the vanishing slope at $r = 0$. As a consequence, the stress $\sigma_{z\varphi}$ is smaller than the microstress $q_{z\varphi}$ in the case $s = 1$, and greater than $q_{z\varphi}$ in the case $s = 2$. Furthermore, the shear stress in the case $s = 2$ is zero at the center of the rod, see (42), while in the case $s = 1$ expression (39) predicts a non-zero value at $r = 0$. For $s = 1$ and $\gamma = 0^+$ (limit to zero from above) the stress is constant and equal to $\sigma_Y^0/\sqrt{3}$, resembling the ultimate (limit) state in the case of classical ideal plasticity. Similar plots can be obtained for other two relations $\sigma_0 = \sigma_0(E_{\rm p})$ from (52).

6. Torque-twist relationship

The torque required to produce a given twist θ can be obtained from the overall moment-equilibrium condition. If the Cauchy stress $\sigma_{z\varphi}$ and the line forces p_φ are used, the expression is (Lubarda, 2016a)

$$T(\theta) = 2\pi \int_{\psi a}^{a} r^2 \sigma_{z\varphi}\, {\rm d}r + 2\pi[a^2 p_\varphi(a) + (\psi a)^2 p_\varphi(\psi a)]\,. \tag{43}$$

If the microstress $q_{z\varphi}$ and the moment-stresses $\tau_{z\varphi r}$ and $\tau_{zr\varphi}$ are used instead (Fig. 6), the expression is

$$T(\theta) = 2\pi \int_{\psi a}^{a} \big[r^2 q_{z\varphi} + r(\tau_{z\varphi r} - \tau_{zr\varphi})\big]{\rm d}r\,. \tag{44}$$

The equivalency of (43) and (44) is easily demonstrated by substituting $q_{z\varphi} = \sigma_{z\varphi} + \tau_{z\varphi r,r}$ from (34) into (44), and by applying the integration by parts to evaluate the integral

$$\int_{\psi a}^{a} r^2 \tau_{z\varphi r,r}\, {\rm d}r = \big(r^2 \tau_{z\varphi r}\big)_{\psi a}^{a} - 2\int_{\psi a}^{a} r\tau_{z\varphi r}\, {\rm d}r\,. \tag{45}$$

Since $p_\varphi(a) = \tau_{z\varphi r}(a)$, $p_\varphi(\psi a) = -\tau_{z\varphi r}(\psi a)$, and $\tau_{zr\varphi} = -\tau_{z\varphi r}$, the torque expression (44) reduces to (43).

The expression (44) was established directly by the consideration of the moment equilibrium. It can also be derived by equating the rate of the external work (per unit length of the tube) with the rate of the internal work, i.e.,

$$\begin{aligned} T\dot\theta &= 2\pi \int_{\psi a}^{a} \big(q_{ij}\dot\epsilon_{ij} + \tau_{ijk}\dot\eth_{ijk}\big) r\, {\rm d}r \\ &= 2\pi \int_{\psi a}^{a} (r q_{z\varphi} + \tau_{z\varphi r} - \tau_{zr\varphi})\dot\theta r\, {\rm d}r\,, \end{aligned} \tag{46}$$

which reproduces (44). The expressions analogous to (26) and (29) were used for the rate-of-strain tensor and its gradient.

We proceed with the evaluation of the torque by using (44). Since, by (33),

$$\tau_{z\varphi r} = \frac{1}{2}\,\frac{(\sqrt{2}l)^s}{r^{s-1}}\, q_{z\varphi}\,, \tag{47}$$

(44) becomes

$$T(\theta) = 2\pi \int_{\psi a}^{a} \frac{r^s + (\sqrt{2}l)^s}{r^{s-2}}\, q_{z\varphi}\, {\rm d}r\,. \tag{48}$$

Upon the substitution of (32) for $q_{z\varphi}$, the following general expression is obtained

$$T(\theta) = \frac{2\pi}{\sqrt{3}} \int_{\psi a}^{a} \sigma_0(E_{\rm p})\big[r^s + (\sqrt{2}l)^s\big]^{1/s} r\, {\rm d}r\,. \tag{49}$$

This can be interpreted as the torque required to twist the solid rod of radius a, minus the torque required to twist by the same amount (θ) the solid rod of radius ψa. The torque's rate of change with the twist θ is

$$\frac{{\rm d}T}{{\rm d}\theta} = \frac{2\pi}{3} \int_{\psi a}^{a} \frac{{\rm d}\sigma_0}{{\rm d}E_{\rm p}}\big[r^s + (\sqrt{2}l)^s\big]^{2/s} r\, {\rm d}r\,. \tag{50}$$

The right-hand sides of (49) and (50) can be evaluated numerically for any s and for any assumed relationship $\sigma_0 = \sigma_0(E_{\rm p})$. The results for $s = 1$ and $s = 2$ can be obtained in closed form. For the three adopted relationships $\sigma_0 = \sigma_0(E_{\rm p})$, this is presented in the next section.

For a thin-walled tube of the mid-radius a_* and the wall-thickness $\delta \ll a_*$, there is a closed-form approximate expression

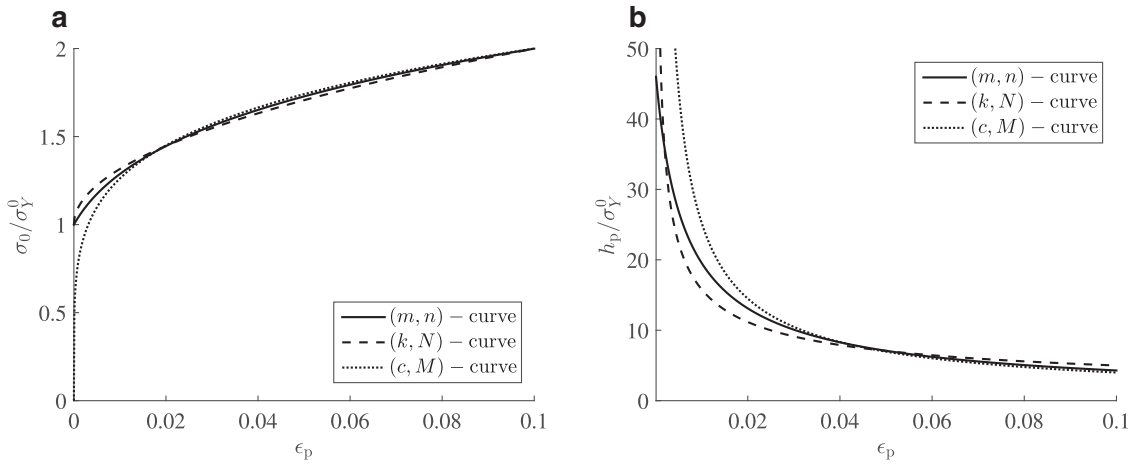

Fig. 7. (a) The comparison of the three stress-strain curves modeling the uniaxial tension test according to (52). The material parameters are ($m = 46.66$, $n = 0.225$), ($k = 3.16$, $N = 0.5$), and ($c = 3.169\,\sigma_Y^0$, $M = 0.2$). (b) The comparison of the corresponding hardening moduli $h_p = d\sigma_0/d\epsilon_p$.

for the torque for any choice of s. This is

$$T(\theta)=\frac{2\pi}{\sqrt{3}}\,a_*\delta\sigma_0(E_p^*)\left[a_*^s+(\sqrt{2}l)^s\right]^{1/s},\quad E_p^*=\frac{\theta}{\sqrt{3}}\left[a_*^s+(\sqrt{2}l)^s\right]^{1/s}, \tag{51}$$

where E_p^* is the gradient-enhanced effective plastic strain evaluated at the mid-radius of the tube $a_* = a - \delta/2 = (1+\psi)a/2$.

7. Closed form expressions for the torque-twist relationship

In this section we derive the torque-twist expression $T = T(\theta)$ for $s = 1$ and $s = 2$, assuming that the stress-strain relationship from uniaxial tension test is modeled by either of the following three expressions

$$\sigma_0(E_p)=\sigma_Y^0\left(1+\frac{m}{n}E_p\right)^n,\quad \sigma_0(E_p)=\sigma_Y^0\left(1+kE_p^N\right),\quad \sigma_0(E_p)=cE_p^M. \tag{52}$$

They are referred to as the relations A, B, and C. The initial yield stress for the first two relations is σ_Y^0, and (m, n), (k, N), and (c, M) are the material constants. The first two relations are modeling a rigid-plastic response; the first of them predicts the initial hardening rate $h_p = m\sigma_Y^0$, while the initial hardening rate according to the second relation is infinitely large. The third relation is not a rigid-plastic type relationship, but a nonlinear elastic type relation, which for the appropriately small values of the exponent M gives a stress-strain curve resembling an elastoplastic response during loading, having a steep response near the zero stress. The comparison of the three stress-strain curves from (52) is shown in Fig. 7a. The material parameters are adjusted so that all three curves give $\sigma_0(0.1) = 2\sigma_Y^0$, which is approximately an increase of stress due to hardening in polycrystalline copper after 10% strain, see experimental data reported in Fleck et al. (1994) and Liu et al. (2013). Fig. 7b shows the comparison of the corresponding hardening moduli $h_p = d\sigma_0/d\epsilon_p$.

7.1. Uniaxial stress-strain relation A

The first considered stress-strain relation from the uniaxial tension test is

$$\sigma_0(E_p)=\sigma_Y^0\left(1+\frac{m}{n}E_p\right)^n,\quad (n\le 1). \tag{53}$$

The parameter $m = h_0/\sigma_Y^0$, where h_0 is the initial hardening rate. By substituting (53) into (49), the torque-twist expression in the case $s = 1$ is found to be

$$T(\theta)=\frac{2\pi}{\alpha^3}\,\frac{\sigma_Y^0}{\sqrt{3}}\left[\frac{\rho^{n+3}}{n+3}-(2+\sqrt{2}l\alpha)\,\frac{\rho^{n+2}}{n+2}+(1+\sqrt{2}l\alpha)\,\frac{\rho^{n+1}}{n+1}\right]_{r=\psi a}^{r=a},\quad (\theta\ne 0), \tag{54}$$

where

$$\rho=1+\alpha(r+\sqrt{2}l),\quad \alpha=\frac{m\theta}{n\sqrt{3}}. \tag{55}$$

For $\theta = 0$, the yield threshold torque is

$$T_Y=T(0)=T_Y^0\left(1+\frac{3}{2}\,\frac{1-\psi^2}{1-\psi^3}\,\frac{\sqrt{2}l}{a}\right),\quad T_Y^0=\frac{2\pi}{3}\,\frac{\sigma_Y^0}{\sqrt{3}}\,(1-\psi^3)a^3. \tag{56}$$

Similarly, in the case $s = 2$ the torque-twist expression is

$$T(\theta)=\frac{2\pi}{\alpha^3}\,\frac{\sigma_Y^0}{\sqrt{3}}\left[\frac{\rho^{n+3}}{n+3}-2\,\frac{\rho^{n+2}}{n+2}+\frac{\rho^{n+1}}{n+1}\right]_{r=\psi a}^{r=a},\quad (\theta\ne 0), \tag{57}$$

where

$$\rho=1+\alpha(r^2+2l^2)^{1/2},\quad \alpha=\frac{m\theta}{n\sqrt{3}}. \tag{58}$$

For $\theta = 0$, the yield torque is

$$T_Y=T(0)=\frac{T_Y^0}{1-\psi^3}\left[\left(1+\frac{2l^2}{a^2}\right)^{3/2}-\left(\psi^2+\frac{2l^2}{a^2}\right)^{3/2}\right],\quad T_Y^0=\frac{2\pi}{3}\,\frac{\sigma_Y^0}{\sqrt{3}}\left(1-\psi^3\right)a^3. \tag{59}$$

7.2. Uniaxial stress-strain relation B

If the uniaxial stress-strain curve is

$$\sigma_0(E_p)=\sigma_Y^0\left(1+kE_p^N\right),\quad (N\le 1), \tag{60}$$

the torque-twist relationship in the case $s = 1$ becomes

$$T(\theta)=\frac{2\pi\sigma_Y^0}{\theta^3}\left[3k\,\frac{E_p^{N+3}}{N+3}-\sqrt{6}lk\theta\,\frac{E_p^{N+2}}{N+2}+E_p^3-\sqrt{\frac{3}{2}}l\theta\,E_p^2\right]_{r=\psi a}^{r=a},\quad E_p=\frac{\theta}{\sqrt{3}}\,(r+\sqrt{2}l). \tag{61}$$

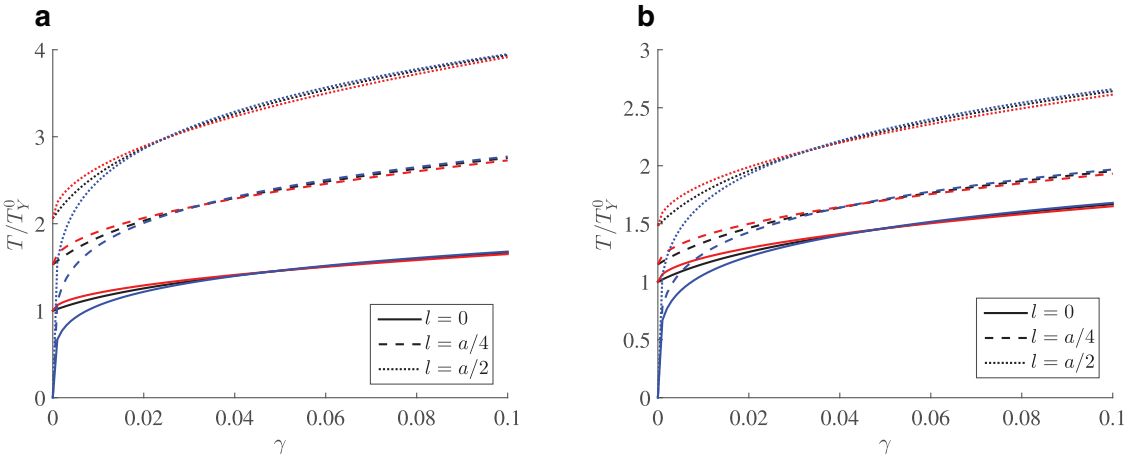

Fig. 8. The variation of the normalized torque T/T_Y^0 with γ for a solid rod with three indicated values of l. The black curves correspond to (m, n) stress-strain curve from Fig. 4a, the red curves to (k, N) curve, and the blue curves for (c, M) curve. (a) Case $s = 1$; (b) Case $s = 2$.

The yield torque is obtained by specifying $\theta = 0$ in (61), which reproduces (56).

In the case $s = 2$, the torque-twist relationship is

$$T(\theta) = \frac{2\pi\sigma_Y^0}{\theta^3}\left[3k\frac{E_p^{N+3}}{N+3} + E_p^3\right]_{r=\psi a}^{r=a}, \quad E_p = \frac{\theta}{\sqrt{3}}(r^2 + 2l^2)^{1/2}. \tag{62}$$

The yield torque is obtained by specifying $\theta = 0$ in (62), which reproduces (59).

7.3. Uniaxial stress-strain relation C

In the strain-gradient analysis of Fleck and Hutchinson (1997), a power-law dependence of the strain energy density on the gradient-enhanced effective strain was assumed, which gives rise to a power-law nonlinear elastic-type relation

$$\sigma_0(E_p) = cE_p^M, \quad (M \le 1). \tag{63}$$

By substituting (63) into (49), the torque expression is found to be

$$T(\theta) = \frac{2\pi c}{\sqrt{3}}\left(\frac{\theta}{\sqrt{3}}\right)^M \int_{\psi a}^{a}\left[r^s + (\sqrt{2}l)^s\right]^{(M+1)/s} r\,dr. \tag{64}$$

This can be integrated in the case $s = 1$ to give

$$T(\theta) = \frac{T^{l=0}(\theta)}{1-\psi^{M+3}}\left[\left(1+\frac{\sqrt{2}l}{a}\right)^{M+3} - \frac{M+3}{M+2}\left(\frac{\sqrt{2}l}{a}\right) \times \left(1+\frac{\sqrt{2}l}{a}\right)^{M+2} + \left(\frac{1}{M+2}\frac{\sqrt{2}l}{a} - \psi\right)\left(\psi + \frac{\sqrt{2}l}{a}\right)^{M+2}\right]. \tag{65}$$

The torque required to produce a twist θ in the absence of strain-gradient effect is

$$T^{l=0}(\theta) = \frac{2\pi ca^3}{\sqrt{3}(M+3)}\left(\frac{a\theta}{\sqrt{3}}\right)^M (1-\psi^{M+3}). \tag{66}$$

Thus, for each ψ, the ratio $T(\theta)/T^{l=0}(\theta)$ is independent of θ, being dependent only on l/a and M.

For a solid rod ($\psi = 0$), the above two expressions reduce to

$$T(\theta) = T^{l=0}(\theta)\left[\left(1+\frac{\sqrt{2}l}{a}\right)^{M+3} - \frac{M+3}{M+2}\left(\frac{\sqrt{2}l}{a}\right) \times \left(1+\frac{\sqrt{2}l}{a}\right)^{M+2} + \frac{1}{M+2}\left(\frac{\sqrt{2}l}{a}\right)^{M+3}\right], \tag{67}$$

and

$$T^{l=0}(\theta) = \frac{2\pi ca^3}{\sqrt{3}(M+3)}\left(\frac{a\theta}{\sqrt{3}}\right)^M. \tag{68}$$

The last two expressions are in agreement with the Fleck and Hutchinson (1997) expression (2.28), apart from the different definition of the gradient-enhanced effective strain and the corresponding material length l. They derived their expression by exploring the assumed homogeneity of the strain energy function and the corresponding torque-twist relationship.

The torque expression in the case $s = 2$, upon integration of (64), is

$$T(\theta) = \frac{T^{l=0}(\theta)}{1-\psi^{M+3}}\left\{\left[1+\left(\frac{\sqrt{2}l}{a}\right)^2\right]^{(M+3)/2} - \left[\psi^2 + \left(\frac{\sqrt{2}l}{a}\right)^2\right]^{(M+3)/2}\right\}, \tag{69}$$

with the same expression for $T^{l=0}(\theta)$ as in (66). For a solid rod ($\psi = 0$), (69) reduces to

$$T(\theta) = T^{l=0}(\theta)\left\{\left[1+\left(\frac{\sqrt{2}l}{a}\right)^2\right]^{(M+3)/2} - \left(\frac{\sqrt{2}l}{a}\right)^{M+3}\right\}, \tag{70}$$

where $T^{l=0}(\theta)$ is given by (68). Expression (70) is equivalent to expression (49) of Liu et al. (2013), and reproduces the Fleck and Hutchinson (1997) expression (2.29), with the adjustment to their definition of the material length l. These authors used experimental data for torsional response of thin copper wires to estimate the value of l that fits the data best. See also the torque-twist integral expression (35) from Huang et al. (2000), obtained by using the mechanism-based strain-gradient plasticity approach of Nix and Gao (1998) and Gao et al. (1999). In the elastoplastic constitutive model used by Gudmundson (2004), the torque-twist relationship was determined numerically from his expressions (56) and (57).

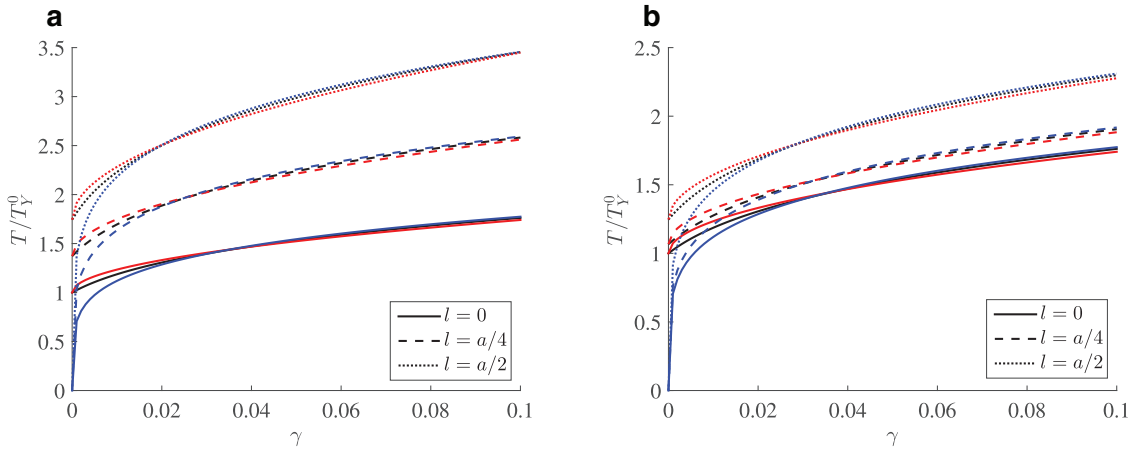

Fig. 9. The variation of the normalized torque T/T_Y^0 with γ for a thin-walled tube of wall-thickness $\delta = a/10$ with three indicated values of l. The black curves correspond to (m, n) stress-strain curve, the red curves to (k, N) curve, and the blue curves for (c, M) curve. (a) Case $s = 1$; (b) Case $s = 2$. (For interpretation of the references to color in this figure legend, the reader is referred to the web version of this article.)

7.4. Numerical results

Fig. 8a shows the variation of the normalized torque T/T_Y^0 with $\gamma = a\theta$ for a solid rod with three indicated values of l in the case $s = 1$. The black curves correspond to (m, n) stress-strain curve from Fig. 7a, the red curves to (k, N) curve, and the blue curves for (c, M) curve. The predicted torque above the strain of about 2% is almost the same, with the differences pronounced below that level of strain. Fig. 8b shows the same in the case $s = 2$. The extent of strain with the notable torque differences is about 3 to 4%. Furthermore, by comparing parts (a) and (b) of Fig. 8 it is observed that the increase of the material length l increases the torque significantly more in the case $s = 1$ than in the case $s = 2$. Fig. 9 shows the results for a thin-walled tube of thickness $\delta = a/10$. The same ratios l/a are used as in Fig. 8, although smaller values may be more appropriate for a thin-walled tube, since δ is the smallest geometric dimension in that case. It may be noted from Figs. 8 and 9 that there is a strong effect of l on the initial yield strength, but relatively small effect on the strengthening rate at sufficiently large values of γ. This is qualitatively in accord with experimental observations by Fleck et al. (1994), who observed the strong influence of the diameter of twisted wires on the yield strength, but relatively small effect on the strain hardening; see also a related discussion by Evans and Hutchinson (2009).

In the case of a thin-walled tube, the analytical results from earlier sections can be simplified by the approximation $\delta/a \ll 1$. For a thin-walled tube, the yield threshold torques in (56) and (59), corresponding to $s = 1$ and $s = 2$, can be also determined from the approximate expression

$$T_Y = T_Y^0\left[1 + \left(\frac{\sqrt{2}l}{a_*}\right)^s\right]^{1/s}, \quad T_Y^0 = 2\pi\,\frac{\sigma_Y^0}{\sqrt{3}}\,a_*^2\delta\,, \tag{71}$$

which follows from (51). The mid-radius of the tube is a_* and the wall-thickness is $\delta \ll a_*$. The plots of (71) corresponding to $\delta = a_*/10$ are shown in Fig. 10. There is a much more pronounced effect of the increase of l/a_* on the increase od T_Y in the case $s = 1$ than $s = 2$. The strain-gradient effects for a thin-walled tube are less pronounced than for a solid rod, because near the center of a solid rod the strain-gradient effects are dominant, the strain itself being there relatively small (or zero at the center). On the other hand, in a thin-walled tube, the strain is nearly constant across the small thickness of the tube and thus dominantly contributes to E_p^* in (51) for $l \ll a_*$. As already pointed out, in fitting experimental data, different values of l may be needed for $s = 1$ and $s = 2$.

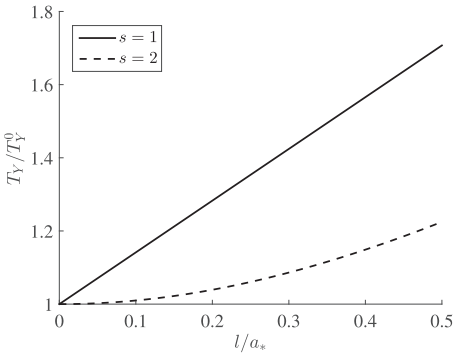

Fig. 10. The variation of the normalized threshold torque T_Y/T_Y^0 with l/a_* for a thin-walled tube of the mid-radius a_* and the wall-thickness $\delta = a_*/10$, according to (71).

The same observations were made in the analysis of twisted solid rods by Fleck and Hutchinson (1997) within their model of strain-gradient plasticity. See also the experimental and theoretical study of size effects in torsion of thin metal wires by Liu et al. (2013).

8. Conclusion

The objective of the present paper was to derive the stress fields and the torque-twist relationship for a hollow circular tube made of a rigid-plastic material with any of the adopted gradient-enhanced effective plastic strain measures from a wide class of these measures defined by (2). The microstress $q_{z\varphi}$ is specified by (32), the moment-stress $\tau_{z\varphi r}$ by (33), and the Cauchy stress $\sigma_{z\varphi}$ by (36). The line forces are also evaluated and discussed from the standpoint of the basic equilibrium considerations and the principle of virtual work, derived in the appendix of the paper. For the two most commonly used measures, defined as a linear and harmonic sum of the effective plastic strain and its gradient ($s = 1$ and $s = 2$), the stress fields are given by (37)–(39) and (40)–(42). The results are plotted in Figs. 4 and 5 for the selected material properties and the chosen material length parameter. In Section 6 we derive a general expression for the torque-twist relationship, given by (49). This is used in Section 7 to obtain the closed-form expressions corresponding to two aforementioned measures of the gradient-enhanced effective plastic strain ($s = 1$ and $s = 2$). Three appealing expressions are adopted to model the stress-strain response in uniaxial tension, listed in (52). The results for selected

values of the material length parameter are shown in Fig. 8 for a solid rod, and in Fig. 9 for a thin-walled tube. The torque required to produce a given amount of twist is significantly more increased by the increase of the material length parameter in the case $s = 1$ than in the case $s = 2$. An approximate expression for the torque is derived for a thin-walled tube, given by (51), which applies for any $s \geq 1$. The corresponding yield threshold value is specified by (71). The results are compared with the related results from the literature. They can be potentially useful for the further studies of the size effect in torsion and the relationship between analytical predictions and experimental observations. The extension of the presented analysis to bending of thin beams is presented in a separate paper (Lubarda, 2016b).

Acknowledgments

Research support from the Montenegrin Academy of Sciences and Arts is kindly acknowledged. I also thank the anonymous reviewers for their helpful comments and suggestions.

Appendix A. Principle of virtual work for rigid-plastic strain-gradient plasticity

For the rigid-plastic material model the virtual plastic strain components are related to the virtual displacement components by

$$\delta\epsilon^{\rm p}_{ij} = \frac{1}{2}\,(\delta u_{i,j} + \delta u_{j,i})\,, \tag{72}$$

since elastic strains are absent. The corresponding principle of virtual work for the strain-gradient plasticity can be cast in the form (Fleck and Willis, 2009b)

$$\int_V \Big(q'_{ij}\delta\epsilon^{\rm p}_{ij} + \tau'_{ijk}\delta\epsilon^{\rm p}_{ij,k} + \frac{1}{3}\,\sigma_{ii}\delta\epsilon^{\rm p}_{jj}\Big){\rm d}V = \int_S \big(T_i\delta u_i + t_{ij}\delta\epsilon^{\rm p}_{ij}\big){\rm d}S\,, \tag{73}$$

provided that the equations of equilibrium hold

$$\sigma_{ij,j} = 0\,, \quad \tau_{ijk,k} + \sigma_{ij} - q_{ij} = 0\,, \tag{74}$$

together with the relations

$$T_i = \sigma_{ij}n_j\,, \quad t_{ij} = \tau'_{ijk}n_k \tag{75}$$

between the traction vector T_i and the Cauchy stress tensor σ_{ij}, and between the (deviatoric) moment-traction tensor t_{ij} are the deviatoric part of the moment-stress tensor τ'_{ijk}. The components of the outward unit vector, orthogonal to the considered surface element, are denoted by n_i. The deviatoric parts of the microstress q_{ij} and the moment-stress τ_{ijk} are defined by

$$q'_{ij} = q_{ij} - \frac{1}{3}\,q_{kk}\delta_{ij}\,, \quad \tau'_{ijk} = \tau_{ijk} - \frac{1}{3}\,\tau_{llk}\delta_{ij}\,. \tag{76}$$

The spherical part of Cauchy stress tensor is usually specified from the equilibrium conditions in conjunction with the traction boundary conditions. The workless spherical parts of the microstress and the moment-stress tensor are included in the analysis for the convenience, and are related to the spherical part of Cauchy stress by $\tau_{jjk,k} + \sigma_{jj} - q_{jj} = 0$. The spherical components of q_{ij} and τ_{ijk} were used in the analysis of pure bending of rigid-plastic beams by Lubarda (2016b).

In view of (72), the second integral on the right-hand side of (73) can be written as

$$\int_S t_{ij}\delta\epsilon^{\rm p}_{ij}\,{\rm d}S = \int_S t_{ij}\delta\left(\frac{\partial u_i}{\partial x_j}\right){\rm d}S = \int_S t_{ij}\frac{\partial(\delta u_i)}{\partial x_j}\,{\rm d}S\,. \tag{77}$$

The variation of the displacement gradient $\delta(u_{i,j})$ over S is not independent of the displacement variation δu_i, because if δu_i is known on S, so is the surface gradient of δu_i (Toupin, 1962; Mindlin, 1964, 1965; Fleck and Hutchinson, 1997). To identify the independent boundary conditions, we then decompose the gradient of the virtual displacement into its surface gradient $D_j(\delta u_i)$ and a normal gradient $n_jD(\delta u_i)$, such that

$$\frac{\partial(\delta u_i)}{\partial x_j} = D_j(\delta u_i) + n_jD(\delta u_i)\,, \tag{78}$$

where

$$D_j = (\delta_{jk} - n_jn_k)\frac{\partial}{\partial x_k}\,, \quad D = n_k\,\frac{\partial}{\partial x_k}\,. \tag{79}$$

Thus, (77) becomes

$$\int_S t_{ij}\delta\epsilon^{\rm p}_{ij}\,{\rm d}S = \int_S t_{ij}D_j(\delta u_i)\,{\rm d}S + \int_S R_iD(\delta u_i)\,{\rm d}S\,, \quad R_i = t_{ij}n_j\,. \tag{80}$$

The first integral on the right-hand side of (80) can be rewritten as

$$\int_S t_{ij}D_j(\delta u_i)\,{\rm d}S = \int_S D_j(t_{ij}\delta u_i)\,{\rm d}S - \int_S D_jt_{ij}\delta u_i\,{\rm d}S\,. \tag{81}$$

Assuming that S is a smooth surface, the application of the surface divergence theorem (Brand, 1947; Toupin, 1962; Mindlin, 1964, 1965) to the first integral on the right-hand side of (81) gives

$$\int_S D_j(t_{ji}\delta u_i)\,{\rm d}S = \int_S (D_kn_k)n_jt_{ji}\delta u_i\,{\rm d}S\,, \quad t_{ji} = t_{ij}\,, \tag{82}$$

so that (80) becomes

$$\int_S t_{ij}\delta\epsilon^{\rm p}_{ij}\,{\rm d}S = \int_S [R_i(D_kn_k) - D_jt_{ij}]\delta u_i\,{\rm d}S + \int_S R_iD(\delta u_i)\,{\rm d}S\,. \tag{83}$$

Consequently, the right-hand side of (73) is

$$\int_S \big(T_i\delta u_i + t_{ij}\delta\epsilon^{\rm p}_{ij}\big){\rm d}S = \int_S [\bar{T}_i\delta u_i + R_iD(\delta u_i)]\,{\rm d}S\,,$$
$$\bar{T}_i = T_i + R_i(D_kn_k) - D_jt_{ij}\,. \tag{84}$$

The number of independent higher-order boundary conditions can be reduced from three to two by incorporating the kinematic restriction on the normal component of $D(\delta u_i)$ on S, imposed by the incompressibility constraint

$$\frac{\partial(\delta u_i)}{\partial u_i} = D_i(\delta u_i) + n_iD(\delta u_i) = 0 \quad \Rightarrow \quad n_iD(\delta u_i) = -D_i(\delta u_i)\,. \tag{85}$$

To incorporate (85) into (84), we first decompose R_i into its component $\hat{R}_i = R_i - n_in_jR_j$, tangential to S, and the component $n_in_jR_j$ normal to S. This gives

$$\int_S R_iD(\delta u_i)\,{\rm d}S = \int_S \hat{R}_iD(\delta u_i)\,{\rm d}S + \int_S (R_jn_j)n_iD(\delta u_i)\,{\rm d}S$$
$$= \int_S \hat{R}_iD(\delta u_i)\,{\rm d}S - \int_S (R_jn_j)D_i(\delta u_i)\,{\rm d}S\,. \tag{86}$$

The second integral on the right-hand side can be recast as

$$\int_S (R_jn_j)D_i(\delta u_i)\,{\rm d}S = \int_S D_i(R_jn_j\delta u_i)\,{\rm d}S - \int_S D_i(R_jn_j)\delta u_i\,{\rm d}S\,. \tag{87}$$

The application of the surface divergence theorem to the first integral on the right-hand side of (87) gives

$$\int_S D_i(R_jn_j\delta u_i)\,{\rm d}S = \int_S (D_kn_k)n_in_jR_j\delta u_i\,{\rm d}S\,. \tag{88}$$

Consequently, (86) becomes

$$\int_S R_i D(\delta u_i)\,\mathrm{d}S = \int_S \hat{R}_i D(\delta u_i)\,\mathrm{d}S - \int_S [(D_k n_k) n_i n_j R_j - D_i(R_j n_j)]\delta u_i\,\mathrm{d}S\,. \tag{89}$$

The final form of the virtual work principle is, therefore,

$$\int_V \left(q'_{ij}\delta\epsilon^{\mathrm{p}}_{ij} + \tau'_{ijk}\delta\epsilon^{\mathrm{p}}_{ij,k} + \frac{1}{3}\sigma_{ii}\delta\epsilon^{\mathrm{p}}_{jj}\right)\mathrm{d}V = \int_S \left[\hat{T}_i\delta u_i + \hat{R}_i D(\delta u_i)\right]\mathrm{d}S\,, \tag{90}$$

where the three independent traction components $\hat{T}_i$ are

$$\hat{T}_i = \bar{T}_i - n_i n_j R_j (D_k n_k) - D_i(n_j R_j)\,, \tag{91}$$

and the two independent higher-order traction components $\hat{R}_i$, tangential to S, are

$$\hat{R}_i = R_i - n_i n_j R_j\,, \quad R_i = t_{ij} n_j\,. \tag{92}$$

As in the analysis of Toupin (1962); Mindlin (1964); 1965), and Fleck and Hutchinson (1997), if the surface S has edges, then for each smooth segment S_n of S, bounded by the curve C_n, the surface divergence theorem (Brand, 1947, eq. (3) on page 222) can be written as

$$\int_{S_n} D_j f_j\,\mathrm{d}S_n = \int_{S_n} (D_k n_k) n_j f_j\,\mathrm{d}S + \oint_{C_n} k_j f_j\,\mathrm{d}C_n\,, \quad f_j = t_{ji}\delta u_i\,, \tag{93}$$

where $\mathbf{k} = \mathbf{c}\times\mathbf{n}$ is the unit outward normal to C_n, tangent to S_n. The unit vector along C_n is denoted by $\mathbf{c}$. This gives rise to line force contribution $\bar{p}_i$ along C_n, and their virtual work

$$\sum_n \oint_{C_n} \bar{p}_i \delta u_i\,\mathrm{d}C_n \tag{94}$$

has to be added to the right-hand side of (84). For example, the line force along an edge formed by the intersection of two smooth surface segments $S^{(1)}$ and $S^{(2)}$ is

$$\bar{p}_i = \tau'_{ijk} k_j^{(1)} n_k^{(1)} + \tau'_{ijk} k_j^{(2)} n_k^{(2)}\,, \tag{95}$$

where $\mathbf{n}^{(i)}$ is the unit outward normal to surface $S^{(i)}$ $(i = 1, 2)$, and $\mathbf{k}^{(i)} = \mathbf{c}^{(i)}\times\mathbf{n}^{(i)}$. The vector $\mathbf{c}^{(i)}$ is the unit tangent vector along the intersecting edge of the two surfaces with $S^{(i)}$ to the left.

Similarly, the surface divergence theorem in (88) is modified, which gives rise to an additional contribution to line forces. Along an edge formed by the intersection of two smooth surface segments $S^{(1)}$ and $S^{(2)}$, this contribution is

$$-\left[k_i^{(1)}\tau'_{jkl} n_j^{(1)} n_k^{(1)} n_l^{(1)} + k_i^{(2)}\tau'_{jkl} n_j^{(2)} n_k^{(2)} n_l^{(2)}\right]. \tag{96}$$

Thus, the total line force p_i along an edge formed by the intersection of two smooth surface segments $S^{(1)}$ and $S^{(2)}$ is the sum of (95) and (96), i.e.,

$$p_i = \left[\tau'_{ijk} k_j^{(1)} n_k^{(1)} - k_i^{(1)}\tau'_{jkl} n_j^{(1)} n_k^{(1)} n_l^{(1)}\right] + \left[\tau'_{ijk} k_j^{(2)} n_k^{(2)} - k_i^{(2)}\tau'_{jkl} n_j^{(2)} n_k^{(2)} n_l^{(2)}\right]. \tag{97}$$

In conclusion, for a body bounded by a peace-wise smooth surface S, the principle of virtual work (90) is expanded to read

$$\int_V \left(q'_{ij}\delta\epsilon^{\mathrm{p}}_{ij} + \tau'_{ijk}\delta\epsilon^{\mathrm{p}}_{ij,k} + \frac{1}{3}\sigma_{ii}\delta\epsilon^{\mathrm{p}}_{jj}\right)\mathrm{d}V = \int_S \left[\hat{T}_i\delta u_i + \hat{R}_i D(\delta u_i)\right]\mathrm{d}S + \sum_n \oint_{C_n} p_i \delta u_i\,\mathrm{d}C_n\,. \tag{98}$$

In the torsion problem considered in the body of the paper, the only nonvanishing traction component is $\hat{T}_\varphi = \sigma_{z\varphi}$ at the ends of the tube, while the line forces are $p_\varphi(a) = \tau_{z\varphi r}(a)$ and $p_\varphi(\psi a) = -\tau_{z\varphi r}(\psi a)$.

References

Anand, L., Gurtin, M.E., Lele, S.P., Gething, M., 2005. A one-dimensional theory of strain-gradient plasticity: formulation, analysis, numerical results. J. Mech. Phys. Solids 53, 1789–1826.

Anand, L., Gurtin, M.E., Reddy, B.D., 2015. The stored energy of cold work, thermal annealing, and other thermodynamic issues in single crystal plasticity at small length scales. Int. J. Plasticity 64, 1–25.

Bardella, L., 2006. A deformation theory of strain gradient crystal plasticity that accounts for geometrically necessary dislocations. J. Mech. Phys. Solids 54, 128–160.

Bardella, L., 2007. Some remarks on the strain gradient crystal plasticity modelling, with particular reference to the material length scales involved. Int. J. Plasticity 23, 296–322.

Bardella, L., Panteghini, A., 2015. Modelling the torsion of thin metal wires by distortion gradient plasticity. J. Mech. Phys. Solids 78, 467–492.

Brand, L., 1947. Vector and Tensor Analysis. John Wiley & Sons, New York (8th printing, 1962).

Dahlberg, C.F.O., Faleskog, J., Niordson, C.F., Legarth, B.N., 2013. A deformation mechanism map for polycrystals modeled using strain gradient plasticity and interfaces that slide and separate. Int. J. Plasticity 43, 177–195.

Engelen, R.A.B., Fleck, N.A., Peerlings, R.H.J., Geers, M.G.D., 2006. An evaluation of higher-order plasticity theories for predicting size effects and localisation. Int. J. Solids Struct. 43, 1857–1877.

Evans, A.G., Hutchinson, J.W., 2009. A critical assessment of theories of strain gradient plasticity. Acta Mater. 57, 1675–1688.

Fleck, N.A., Hutchinson, J.W., 1993. A phenomenological theory for strain gradient effects in plasticity. J. Mech. Phys. Solids 41, 1825–1857.

Fleck, N.A., Hutchinson, J.W., 1997. Strain gradient plasticity. Adv. Appl. Mech. 33, 295–361.

Fleck, N.A., Hutchinson, J.W., 2001. A reformulation of strain gradient plasticity. J. Mech. Phys. Solids 49, 2245–2271.

Fleck, N.A., Hutchinson, J.W., Willis, J.R., 2014. Strain gradient plasticity under non-proportional loading. Proc. Roy. Soc. A 470, 20140267.

Fleck, N.A., Hutchinson, J.W., Willis, J.R., 2015. Guidelines for constructing strain gradient plasticity theories. J. Appl. Mech. 82, 071002.

Fleck, N.A., Muller, G.M., Ashby, M.F., Hutchinson, J.W., 1994. Strain gradient plasticity: theory and experiment. Acta Metall. Mater. 42, 475–487.

Fleck, N.A., Willis, J.R., 2009a. A mathematical basis for strain gradient plasticity theory. Part I: scalar plastic multiplier. J. Mech. Phys. Solids 57, 161–177.

Fleck, N.A., Willis, J.R., 2009b. A mathematical basis for strain gradient plasticity theory. Part II: tensorial plastic multiplier. J. Mech. Phys. Solids 57, 1045–1057.

Gao, H., Huang, Y., Nix, W.D., Hutchinson, J.W., 1999. Mechanism-based strain gradient plasticity – i. theory. J. Mech. Phys. Solids 47, 1239–1263.

Gudmundson, P.A., 2004. Unified treatment of strain gradient plasticity. J. Mech. Phys. Solids 52, 1379–1406.

Gurtin, M.E., 2002. A gradient theory of single-crystal viscoplasticity that accounts for geometrically necessary dislocations. J. Mech. Phys. Solids 50, 5–32.

Gurtin, M.E., 2003. On a framework for small-deformation viscoplasticity: free energy, microforces, strain gradients. Int. J. Plasticity 19, 47–90.

Gurtin, M.E., 2004. A gradient theory of small-deformation isotropic plasticity that accounts for the burgers vector and for dissipation due to plastic spin. J. Mech. Phys. Solids 52, 2545–2568.

Gurtin, M.E., Anand, L., 2005a. A theory of strain-gradient plasticity for isotropic, plastically irrotational materials. Part I: small deformations. J. Mech. Phys. Solids 53, 1624–1649.

Gurtin, M.E., Anand, L., 2005b. A theory of strain-gradient plasticity for isotropic, plastically irrotational materials. Part II: finite deformations. J. Mech. Phys. Solids 53, 2297–2318.

Gurtin, M.E., Anand, L., 2009. Thermodynamics applied to gradient theories involving accumulated plastic strain. the theories of Aifantis and Fleck and Hutchinson and their generalizations. J. Mech. Phys. Solids 57, 405–421.

Huang, Y., Gao, H., Nix, W.D., Hutchinson, J.W., 2000. Mechanism-based strain gradient plasticity - II. analysis. J. Mech. Phys. Solids 48, 99–128.

Huang, Y., Qu, S., Hwang, K.C., Li, M., Gao, H., 2004. A conventional theory of mechanism-based strain gradient plasticity. Int. J. Plast. 20, 753–782.

Hutchinson, J.W., 2000. Plasticity at the micron scale. Int. J. Solids Struct. 37, 225–238.

Hutchinson, J.W., 2012. Generalizing j_2 flow theory: fundamental issues in strain gradient plasticity. Acta Mech. Sinica 28, 1078–1086.

Idiart, M.I., Deshpande, V.S., Fleck, N.A., Willis, J.R., 2009. Size effects in the bending of thin foils. Int. J. Eng. Sci. 47, 1251–1264.

Liu, D., He, Y., Dunstan, D.J., Zhang, B., Gan, Z., Hu, P., 2013. Toward a further understanding of size effects in the torsion of thin metal wires: an experimental and theoretical assessment. Int. J. Plasticity 41, 30–52.

Lubarda, V.A., 2016a. On the recoverable and dissipative parts of higher order stresses in strain gradient plasticity. Int. J. Plasticity 78, 26–43.

Lubarda, V. A., 2016b. On the analysis of pure bending of rigid-plastic beams in strain-gradient plasticity Submitted.

Mindlin, R.D., 1964. Micro-structure in linear elasticity. Arch. Ration. Mech. Anal. 16, 51–78.

Mindlin, R.D., 1965. Second gradient of strain and surface tension in finite elasticity. Int. J. Solids Struct. 1, 417–438.

Nielsen, K.L., Niordson, C.N., 2014. A numerical basis for strain gradient plasticity theory: rate-independent and rate-dependent formulations. J. Mech. Phys. Solids 63, 113–117.
Nix, W.D., Gao, H., 1998. Indentation size effects in crystalline materials: a law for strain gradient plasticity. J. Mech. Phys. Solids 46, 411–425.
Polizzotto, C., 2009. A nonlocal strain gradient plasticity theory for finite deformations. Int. J. Plasticity 25, 1280–1300.
Polizzotto, C., 2010. Strain gradient plasticity, strengthening effects and plastic limit analysis. Int. J. Solids Struct. 47, 100–112.
Polizzotto, C., 2011. Size effects on the plastic collapse limit load of thin foils in bending and thin wires in torsion. Eur. J. Mech. A/Solids 30, 854–864.
Stölken, J.S., Evans, A.G., 1998. A microbend test method for measuring the plasticity length scale. Acta mater. 46, 5109–5115.
Toupin, R.A., 1962. Elastic materials with couple stresses. Arch. Ration. Mech. Anal. 11, 385–414.
Voyiadjis, G.Z., Abu Al-Rub, R.K., 2005. Gradient plasticity theory with a variable length scale parameter. Int. J. Solids Struct. 42, 3998–4029.
Voyiadjis, G.Z., Pekmezi, G., Deliktas, B., 2010. Nonlocal gradient-dependent modeling of plasticity with anisotropic hardening. Int. J. Plasticity 26, 1335–1356.